Journal of Solid State Chemistry 187 (2012) 64–69

Contents lists available at SciVerse ScienceDirect

Journal of Solid State Chemistry

journal homepage: www.elsevier.com/locate/jssc

Atomic Pt and molecular H_2O adsorptions on $SrTiO_3$ with and without Nb-doping: Electron trapping center and mediating roles of Pt in charge transfer from semiconductor to water

Wei Wei, Ying Dai*, Meng Guo, Yandong Ma, Baibiao Huang

School of Physics, State Key Laboratory of Crystal Materials, Shandong University, Shanda South Road 27, Jinan 250100, People's Republic of China

ARTICLE INFO

Article history:
Received 25 August 2011
Received in revised form
19 December 2011
Accepted 23 December 2011
Available online 3 January 2012

Keywords:
$SrTiO_3$ (0 0 1) surface
Pt adsorption
H_2O adsorption
Charge transfer
DFT calculation

ABSTRACT

H_2O adsorption on SrO-terminated $SrTiO_3$ (0 0 1) surface has been investigated with the first-principles calculation based on DFT. An energy barrier of 0.221 eV for H_2O dissociation is obtained, which illustrates a spontaneous dissociation. H and O atoms on the SrO-termination of (0 0 1) surface recombine readily. It demonstrates that Pt induces surface dipole moment and changes the surface work function. Adsorption of atomic Pt on SrO-termination of Nb-doped $SrTiO_3$ (0 0 1) surface indicates charge transfer from the surface to Pt, i.e., Pt is negatively charged. Fukui functions illustrate the role Pt played in mediating charge transfer from (0 0 1) surface to targets adsorbed on Pt. H_2O adsorption on the Pt atom supported on Nb-doped $SrTiO_3$ confirms the charge transfer from semiconductor containing electrons to target species, which is mediated by metal. Charge transfer from negatively charged Pt to H_2O weakens (activates) the H–O bonds in molecule H_2O.

1. Introduction

As a promising photocatalyst material, perovskite-type $SrTiO_3$ has been attracting more and more attention due to its excellent performance in decomposing organic compounds and overall water splitting for H_2/O_2 evolution [1–11]. However, because of its wide band gap (about 3.2 eV [12,13]), $SrTiO_3$ can only absorb a small portion in the ultraviolet (UV) region, which accounts for less than 5% of the solar spectrum in energy. This greatly restricts its photocatalytic efficiency. To improve the efficiency, doping foreign elements in the host for the sake of making $SrTiO_3$ visible light-driven has been investigated as an important approach in experiments and in theory as well [14–19]. Although orbital insertion in the band gap makes $SrTiO_3$ response to visible light, it does not definitely guarantee photocatalytic activity under the visible light. Induced in-gap states play as electron–hole pair recombination center. Nonmetal (e.g., nitrogen) doping in $SrTiO_3$ results in narrowed band gap and makes the $SrTiO_3$ visible light-driven, nevertheless, it requires relatively high dopant concentration [1]. Besides, it has been identified that depositing metal nanoparticles on photocatalyst surface can improve the photocatalytic activity because loaded metals reduce the recombination of photogenerated electron–hole pairs. In addition to Au [20], Ag [21] and Pd [22], platinum is also one of the popular candidates. In the quest of high photocatalytic efficiency, Pt is loaded on the photocatalyst surface as a co-catalyst to improve the segregation of photoexcited electron–hole pairs. It has been found that Pt plays an important role in experimental waste oxidation and H_2 generation [23–26]. Water splitting for H_2 generation upon Pt/$SrTiO_3$ (Cr–Ta-doped) composite system was experimentally investigated and it was for the first time that the stoichiometric water splitting (H_2:O_2=2) occurred over semiconductor photocatalyst under visible light [27]. It is speculated that the loaded Pt acts as a H_2 evolution site because Pt has the lowest over-voltage for hydrogen production in H_2O electrolysis. Moreover, Puangpetch et al. [11] verified that an optimum Pt loading of 0.5 wt% on the mesoporous-assembled $SrTiO_3$ demonstrated high H_2 production activity. When metal is precipitated on an n-type semiconductor, it gives rise to a Schottky barrier at the interface region. Since the work function of metal is higher than that of semiconductor, photogenerated electrons in the conduction band of the semiconductor are believed to readily transfer to the metal until the Fermi levels of metal and semiconductor are aligned [28]. What is more, shift of Fermi levels can improve the energetics of the metal/semiconductor composite system as well as the efficiency of interfacial electron transfer process [28,29]. As a consequence, the metal serves as an efficient electron trapping center and prevents the electron–hole pairs from recombination. Nevertheless, study about metal-mediated charge transfer from electronically excited photocatalyst to target species is still in need.

* Corresponding author. Fax: +86 531 88365569.
E-mail address: daiy60@sina.com (Y. Dai).

0022-4596/$ - see front matter © 2012 Elsevier Inc. All rights reserved.
doi:10.1016/j.jssc.2011.12.030

Although it is of importance, little is known at the microscopic level concerning the H_2O adsorption and dissociation properties on the $SrTiO_3$ surface. As a consequence, it is fundamental interest to study the H_2O adsorption properties on $SrTiO_3$ surface. Since the air-stable $SrTiO_3$ (0 0 1) surface has been prepared [30] and most of the experimental and theoretical investigations are carried out upon the (0 0 1) surface [31–36], we choose it as a model to study the adsorption properties in the current work. $SrTiO_3$ (0 0 1) surface bears two terminations, TiO_2- and SrO-termination, and the grand thermodynamic potential F suggests that SrO-terminated (0 0 1) surface is more stable than the TiO_2-terminated one [37,38]. As a consequence, we employ the SrO-termination of $SrTiO_3$ (0 0 1) surface to study the metal adsorption, H_2O adsorption and dissociation and metal-mediated charge transfer. The transition state (TS) of H_2O dissociation on the SrO-termination and the activation barrier are addressed. Contact character between Pt and $SrTiO_3$ (0 0 1) surface with SrO-termination is also described in detail in the current work. The adsorption configuration, adsorption energy, bonding character on the surface and change in surface work function are investigated. Moreover, demand for investigation about the mediating role metal played in storing and shutting photoinduced electrons from the photocatalyst to target species continues to rise. As a matter of fact that Pt plays a role as a reduction site on n-type semiconductor surface [39] and Nb-doped $SrTiO_3$ is generally considered as an n-type semiconductor [40–43], we also examine the Pt adsorption properties on the SrO-termination of Nb-doped $SrTiO_3$ (0 0 1) surface in the present work. Then the trapping center role Pt played can be verified from the adsorption on Nb-doped $SrTiO_3$, while the mediating role Pt played in charge transfer is examined through H_2O adsorption on the negatively charged Pt supported on the SrO-termination of Nb-doped $SrTiO_3$. What is more, as we know that the conduction band of $SrTiO_3$ is mainly composed of Ti 3*d* states and the excess electrons derived from Nb-doping reduce Ti ion from Ti^{4+} to Ti^{3+} [44]. In other words, extra electrons derived from Nb-doping are mainly localized at the conduction band of $SrTiO_3$ and electron-doping in $SrTiO_3$ can be simulated via Nb-doping to simulate the electronic excitation (by photons).

2. Computational method

The first-principles spin-polarized calculations were performed by the Vienna ab initio Simulation Package (VASP) [45,46] based on density functional theory (DFT). The ion–electron interaction was described by projector augmented wave (PAW) [47] pseudopotential and generalized gradient approximation (GGA) in the formulation of Perdew–Burke–Ernzerhof (PBE) functional was employed to treat the exchange and correlation potential [48,49]. The electron wave functions were expanded into a basis set of plane waves with a kinetic energy cutoff of 400 eV. Geometry relaxation was carried out until the residual forces acting on each ion converged within 10^{-2} eV/Å and the convergence threshold for self-consistence-field iteration was set at 10^{-4} eV. A Γ-centered $4\times4\times1$ Monkhorst–Pack mesh of k points was used to sample the Brillouin zone integration.

SrO-terminated $SrTiO_3$ (0 0 1) surface is simulated using the periodic slab method. A slab model consisting of seven alternating atomic layers (SrO–TiO_2– … TiO_2–SrO) with mirror-symmetry and (2×2) periodicity of surface unit cell is employed, as shown in Fig. 1. It should be mentioned that seven atomic layers are sufficient to simulate the adsorption properties on $SrTiO_3$ (0 0 1) surface [50]. The slab model is separated by a vacuum spacing of 23 Å in order to wipe out the interaction between two periodic images. In our calculations the relaxed lattice constant of bulk $SrTiO_3$ is 3.927 Å, which is in agreement with that acquired in previous experiment and DFT calculation [51,52]. The obtained lattice constant was maintained frozen and the three bottom layers of the slab were fixed in their bulk parameters during atomic position relaxation. The upper four layers and the adsorbate were fully relaxed. For a single Pt atom adsorption on this (2×2) (0 0 1) surface, it corresponded to metal coverage of 0.25 monolayer (ML). Electron-doing in $SrTiO_3$ was simulated through substitutional Nb-doping for Ti in the slab model. In the current work, a Ti atom was replaced by a Nb atom, which corresponds to a doping concentration of ~1.47 at%, or to a Nb:Ti ratio of 1:12. The total energies of a free molecule H_2O and a free Pt atom were calculated within a cubic box of side length 15 Å. Surface dipole moment induced by Pt adsorption was taken into account with dipole correction in our calculations [53].

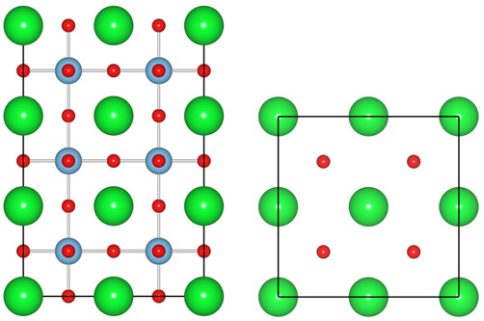

Fig. 1. Slab model of $SrTiO_3$ (0 0 1) surface with SrO-termination. Left panel, side view; right panel, top view of the SrO-termination. The vacuum spacing is 19 Å. The big (green), midsize (gray) and small (red) spheres represent Sr, Ti and O atoms, respectively. (For interpretation of the references to color in this figure legend, the reader is referred to the web version of this article.)

Adsorption energy, E_{ads}, is usually calculated to inspect the stability of adsorption based on the following equation:

$$E_{ads} = E_{(sub+adsorbate)} - E_{sub} - E_{adsorbate}$$

where $E_{(sub+adsorbate)}$, E_{sub} and $E_{adsorbate}$ are the calculated total energies of the substrate with adsorbate thereon, substrate and adsorbate in gas-phase, respectively. Negative adsorption energy implies exothermic adsorption. The more negative the adsorption energy, the more favorable the adsorption should be. The TS for H_2O dissociation was determined through the climbing-image nudged elastic band (CI-NEB) method [54] and the potential energy surface (PES) was constructed accordingly.

3. Results and discussion

3.1. $H_2O/SrTiO_3$

We examine a series of H_2O adsorption configurations on the $SrTiO_3$ (0 0 1) surface and the most preferred configuration of molecular adsorption is shown in Fig. 2(a). As can be noticed, the H–O–H molecular plane is perpendicular to the surface showing a bidentate configuration. Two H atoms converge to two adjacent surface O atoms and the distances between H and O are 1.643 and 1.644 Å. The bond lengths of hydroxyls in the adsorbed molecule H_2O are 1.028 and 1.031 Å, respectively, which are slightly longer than the H–O bond in molecule H_2O in gas-phase (0.973 Å). This demonstrates that the original H–O bonds in adsorbed H_2O stretch in the direction of in-plane O and they are activated. The adsorption energy of molecular H_2O adsorption on the SrO-termination of $SrTiO_3$ (0 0 1) surface is −0.901 eV indicating that the adsorption is exothermic. For H_2O molecular adsorption on

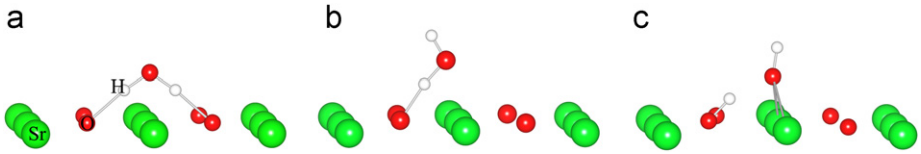

Fig. 2. Energetically preferred adsorption configurations for (a) molecular; (b) TS; and (c) dissociative H_2O on SrO-terminated $SrTiO_3$ (0 0 1) surface ($H_2O/SrTiO_3$). Only the first layer (SrO) of the slab is shown, and the Sr, O, H atoms are labeled.

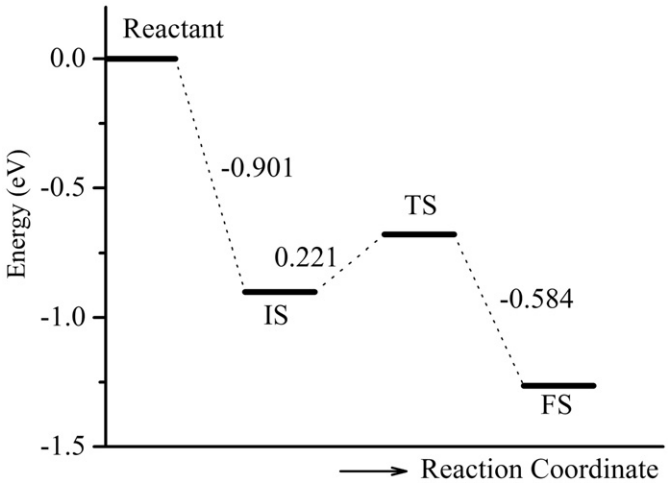

Fig. 3. Potential energy surface constructed for H_2O adsorption and dissociation on the SrO-terminated $SrTiO_3$ (0 0 1) surface. IS represents molecular H_2O adsorption and FS represents dissociative H_2O adsorption. IS and FS correspond to the configurations shown in Fig. 2(a) and (c), respectively.

the TiO_2-termination [55], the oxygen atom of H_2O bonds to a surface Ti atom and the adsorption energy is calculated to be −0.834 eV. In order to see the dissociation of H_2O, we further check the dissociative adsorption of H_2O on SrO-terminated $SrTiO_3$ (0 0 1) surface. The energetically most preferred configuration is shown in Fig. 2(c). It can be seen that one H–O bond breaks and the ruptured H atom is bonded to one adjacent surface O atom. Bond length of this derivative hydroxyl on the surface is 1.010 Å, which is slightly longer than that in the gas-phase H_2O. This shows a strong interaction between the H and surface O atom. OH complex of the dissociative H_2O shifts away from the on-surface H with the O atom locating at a bridge site between two surface Sr atoms. The two hydroxyl groups are strongly tilted each other, which can be seen from Fig. 2(c). Distances between the O and the surface Sr atoms are 2.549 and 2.608 Å, which are comparable with that in rock salt SrO (2.565 Å). This dissociative adsorption is thermodynamically favored on the (0 0 1) surface. The adsorption energy is −1.264 eV, which is more negative than that of molecular adsorption. Dissociative H_2O adsorption properties revealed in our present work also reflect the observation in experiment that hydroxyl emerges on the SrO-termination of $SrTiO_3$ (0 0 1) surface [56]. Whereafter, we address the TS for the dissociation from molecular adsorbed H_2O (Fig. 2(a)) into a hydroxyl group and a proton (Fig. 2(c)) on the SrO-termination. As can be seen from the configuration TS shown in Fig. 2(b), H_2O initially rotates with one of its H atoms going away form the surface. Whereafter, one H–O bond breaks with one H toward the surface O atom. The corresponding reaction PES is depicted in Fig. 3. It can be noticed that the potential energy of this TS is −0.680 eV, which is more negative than that of the reactant. This demonstrates that net activation energy is not demanded for H_2O dissociation on the surface. This means that H_2O dissociation takes place spontaneously upon the SrO-terminated $SrTiO_3$ (0 0 1) surface, namely, the released energy can be used to overcome the

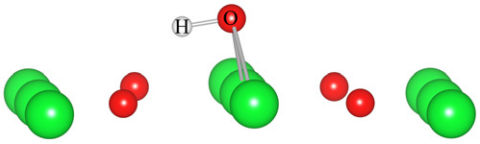

Fig. 4. OH adsorption on the SrO-termination of $SrTiO_3$ (0 0 1) surface ($OH/SrTiO_3$). Only the first layer (SrO) of the slab is shown and the OH complex is denoted.

energy barrier for this H_2O partial dissociation. In other words, H_2O can hardly exist as an intact molecule on the SrO-termination of $SrTiO_3$ (0 0 1) surface. The activation barrier is calculated to be 0.221 eV, which is obviously smaller than the released energy (0.363 eV) in the dissociation. For H_2O dissociative adsorption on the $SrTiO_3$ (0 0 1) surface with TiO_2-termination [55], it indicates that the OH is located on a Ti atom and the H on an adjacent O atom. The adsorption energy is calculated to be −0.922 eV. The energy barrier for H_2O dissociation on the TiO_2-termination is 0.204 eV, which is comparable to that on the SrO-termination.

In addition, we examine the adsorption and dissociation of an OH complex on the SrO-terminated $SrTiO_3$ (0 0 1) surface. It cannot obtain a dissociative formation of OH, separated H and O, on the SrO-termination. This means that water dissociation on the SrO-termination is a one-step reaction. In other words, H and O atoms readily recombine and exit as an OH complex on the SrO-termination of (0 0 1) surface. This may reduce the yielding of H_2. The adsorption configuration of $OH/SrTiO_3$ is shown in Fig. 4. The bond length of this hydroxyl is 0.980 Å. The O atom in the OH complex is located over two surface Sr atoms and the distances between O and surface Sr are both 2.467 Å.

3.2. *$Pt/SrTiO_3$ and $Pt/SrTiO_3$:Nb*

A metal deposition on oxide substrates begins with the adsorption of isolated atoms, which is the initial stage of metal atom clustering and metal film growth. Study about a single atom adsorption is useful to understand the contact behavior between metals and oxide photocatalysts. Also, the mediating role metal played in charge transfer can be modeled via a single atom.

A series of adsorption configurations of a Pt atom at the high-symmetry sites on the SrO-terminated $SrTiO_3$ (2×2) (0 0 1) surface are examined. The most stable adsorption configuration is available from Fig. 5(a) (denoted as $Pt/SrTiO_3$), from which it can be noticed that the Pt atom is adsorbed to a surface O atom with the adsorption energy of −3.189 eV. This Pt–O bond tilts toward the surface and the bond length is calculated to be 1.926 Å. In order to study the bonding nature between Pt and the SrO-termination, total density of states (DOS) of the first SrO layer of the substrate and projective DOS on Pt are depicted in Figs. 6(a) and (b), respectively. It can be found out that some localized gap states appear above the valence band, which are dominantly composed of hybridized Pt 5*d* and O 2*p* states. It demonstrates that both Pt 5*d* and 6*s* states show nonspin-polarization. In experimental observation, Pt-loaded $SrTiO_3$ represents photocatalytic activity under visible light [11,27]. Accordingly, introduction of in-gap states is a possible reason for the

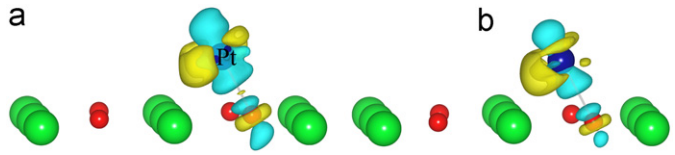

Fig. 5. Charge density difference for atomic Pt adsorption on the SrO-termination of (0 0 1) surface of (a) pristine $SrTiO_3$ (Pt/$SrTiO_3$); (b) Nb-doped $SrTiO_3$ (Pt/$SrTiO_3$:Nb). The cyan region represents charge depletion, and the yellow region represents charge accumulation; the isosurface value is 0.01 e/Å^3. Only the first layer (SrO) of the slab is shown and the Pt atom is labeled. (For interpretation of the references to color in this figure legend, the reader is referred to the web version of this article.)

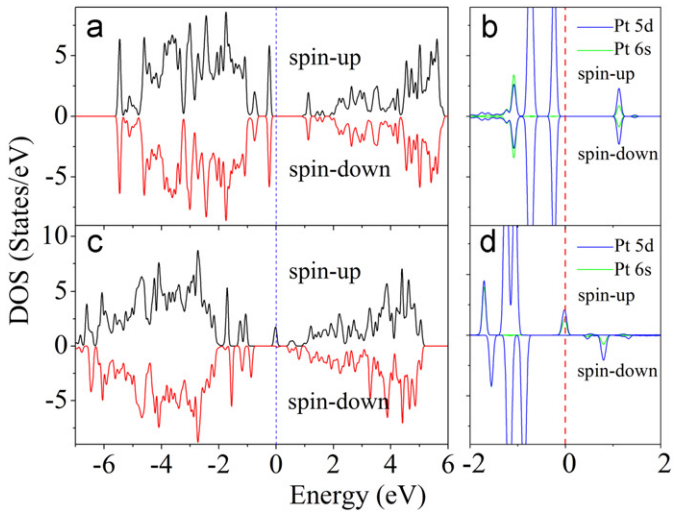

Fig. 6. Density of states (DOS) plotted for a single Pt atom adsorbed on the $SrTiO_3$ (0 0 1) surface with SrO-termination. (a) and (c) are total DOS of the first SrO layer of Au/$SrTiO_3$ and Au/$SrTiO_3$:Nb, respectively; (b) and (d) are the projective DOS of adsorbed Au atom on Au/$SrTiO_3$ and Au/$SrTiO_3$:Nb, respectively. The dotted vertical lines represent the Fermi level.

visible light response. Our results resemble that of previous first-principles calculation about Pt adsorption on $SrTiO_3$ (1 0 0) surface with respect to adsorption energy, Pt–O bond length and bonding character [57].

In order to characterize the charge redistribution behavior at the interface in detail, we examine the charge density difference according to the following equation:

$$\Delta\rho(\mathbf{r}) = \rho^{\mathrm{Pt/sub}}(\mathbf{r}) - \rho^{\mathrm{sub}}(\mathbf{r}) - \rho^{\mathrm{Pt}}(\mathbf{r})$$

where $\rho^{\mathrm{Pt/sub}}(\mathbf{r})$ is the charge density of the complete adsorption system; $\rho^{\mathrm{sub}}(\mathbf{r})$ and $\rho^{\mathrm{Pt}}(\mathbf{r})$, respectively, represents the charge density of bare substrate and adsorbate. $\rho^{\mathrm{sub}}(\mathbf{r})$ and $\rho^{\mathrm{Pt}}(\mathbf{r})$ are calculated in the configurations as that in the relaxed composite system Pt/$SrTiO_3$. As shown in Fig. 5(a), lack of electron density accumulation in the region between Pt and SrO-termination illustrates that intraunit polarization predominantly contributes to the bonding mechanism of the Pt–O. Charge redistribution is restricted to Pt and O and the rest of the surface remains unperturbed, which reveals the local nature of this Pt–O bond. Furthermore, there is still little charge is localized on the Pt–O bond indicating weak covalent components of the Pt–O bond.

It has been identified that electric dipole induced by charge transfer at the interface of metal/substrate changes the surface work function [58]. To distinctly demonstrate the work function change, dipole correction is taken into account in our calculations. Fig. 7 indicates the average electrostatic potential in the plane parallel to (0 0 1) surface along [0 0 1] direction, in which the work function change ($\Delta\Phi$, in eV) is defined. The surface work

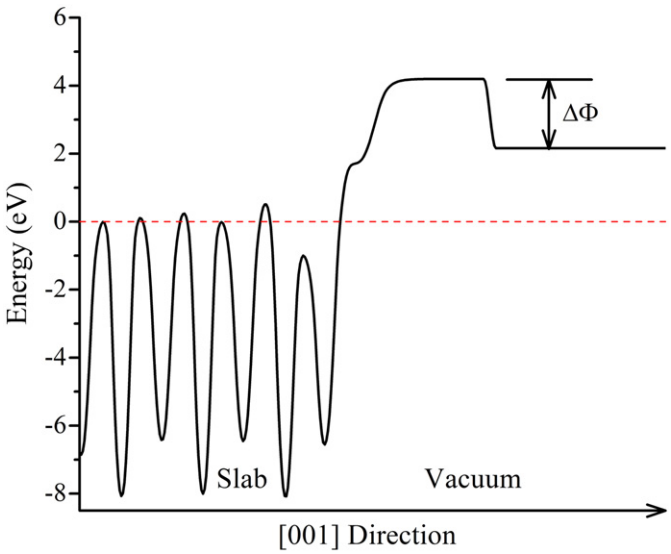

Fig. 7. The electrostatic potential averaged in the plane parallel to the (0 0 1) surface along the [0 0 1] direction for Pt atom adsorption on SrO-terminated $SrTiO_3$ (2 × 2) (0 0 1) surface (Pt/$SrTiO_3$); $\Delta\Phi$ is defined as the change in work function and the horizontal dashed line represents the Fermi level.

function is defined as the difference between the vacuum level and the Fermi level. As a result of the dipole correction, two well-defined work functions are indicated and the potential drop (i.e. $\Delta\Phi$) is presented in the vacuum level in Fig. 7. One of the work functions is for the side of slab with Pt atom adsorbed thereon, while the other one is for the bare side of the slab (the nearest periodic image cell). As usually adopted in surface calculation, accordingly, there are two manners to calculate the change in work function: (1) the slab is not centered in the cell and the bottom layers are frozen during structure relaxation (as the present work), work function change can be obtained by calculating the work function difference between the adsorbed system and the full relaxed substrate without adsorbate thereon; (2) the slab is centered in the cell and the central layers are frozen during structure relaxation, the work function change is represented by the potential drop as shown in Fig. 7 (on the premise that the slab is of mirror-symmetry). For atomic Pt adsorption on SrO-terminated $SrTiO_3$ (2 × 2) (0 0 1) surface, the work function change is calculated to be 0.626 eV. According to the Helmholtz equation, surface dipole moment (in Debye) can be acquired [59] as follows:

$$\mu = (1/12\pi)A\Delta\Phi/\Theta$$

where A is the area in Å^2 per (1 × 1) surface unit cell and Θ is the metal overage. For a Pt atom adsorption on SrO-terminated $SrTiO_3$ (2 × 2) (0 0 1) surface, dipole moment of 1.024 D is obtained.

To check the dependence of adsorption properties on metal coverage, we examine a single Pt atom adsorption on SrO-terminated $SrTiO_3$ (0 0 1) surface with (1 × 1) and (2 × 1) periodicity of surface unit cell. This, respectively, corresponds to the coverage of 1 and 0.5 ML. In order to obtain more accurate results in calculations, k points were improved to 8 × 8 × 1 for the former and 6 × 6 × 1 for the later. In both cases, it reveals that Pt atom bonds to a surface oxygen atom. It means that O atom is still the active site for Pt adsorption. The adsorption energy E_{ads}, Pt–O bond length $d_{\mathrm{Pt-O}}$, work function change $\Delta\Phi$ and surface dipole moment μ are summarized in Table 1. It can be found that E_{ads} increases somewhat with metal coverage increasing, which implies weak repulsive interaction between adatoms [60]. Pt–O bond length indicates a weak increase with metal coverage increasing. Surface work function is changed due to the induced

Table 1
Pt coverage Θ (ML), adsorption energy E_{ads} (eV), Pt–O bond length d_{Pt-O} (Å), change in work function $\Delta\Phi$ (eV) and surface dipole moment μ (D) for atomic Pt adsorption on the SrO-termination of $SrTiO_3$ (0 0 1) surface (Pt/$SrTiO_3$).

Θ (ML)	E_{ads} (eV)	D_{Pt-O} (Å)	$\Delta\Phi$ (eV)	μ (D)
0.25	−3.189	1.926	0.626	1.024
0.5	−2.953	1.932	0.497	0.407
1	−2.886	1.941	0.532	0.218

surface dipole moment, which appears to depolarize, namely, induced surface dipole moment μ decreases with metal coverage increasing.

We now turn to the atomic Pt adsorption properties on electron-doped $SrTiO_3$. The electron-doped $SrTiO_3$ is simulated by substituting a Nb atom for one Ti atom (in the first TiO_2 layer of the slab, refer to Fig. 1, denoted as $SrTiO_3$:Nb) in the slab model. Previously reported formation energy indicates that the Nb atom energetically prefers to substitute Ti atom in Nb-doped $SrTiO_3$ [44]. For a single Pt atom adsorption on the SrO-terminated (0 0 1) surface of $SrTiO_3$:Nb (denoted as Pt/$SrTiO_3$:Nb), it illustrates a similar adsorption configuration with Pt/$SrTiO_3$. Pt–O bond length is 2.043 Å and the adsorption energy is −3.241 eV, both of which are changed a little compared with that of Pt/$SrTiO_3$. The total DOS of the first SrO layer of Pt/$SrTiO_3$:Nb model and the projective DOS on Pt are depicted in Figs. 6(c) and (d), respectively. It implies that more Pt states are occupied compared with that in the case of Pt/$SrTiO_3$ and Pt states appears to be spin-polarized. This indicates that extra charge from Nb-doping further transfers to Pt. Pt *d*-band center shifts away from the Fermi level compared with that of Pt in Pt/$SrTiO_3$. So, the activity of Pt to molecule is reduced. This can be confirmed by H_2O adsorption energies on Pt/$SrTiO_3$ and Pt/$SrTiO_3$:Nb, which will be discussed later. Charge density difference for Pt/$SrTiO_3$:Nb is shown in Fig. 5(b), from which it can be noticed that charge density accumulates around the Pt atom, i.e., the Pt atom is formally negatively charged. This obviously shows the charge transfer at the interface region from electron-doped $SrTiO_3$ to Pt due to the relatively high electron affinity of Pt (EA_{Pt}=2.13 eV). From above, electron trapping center role loaded-metal played can be addressed. For photocatalytic reaction, it demonstrates that photoinduced electrons transfer from photocatalyst to metal. The negatively charged Pt is considered to play a mediating role in storing and shutting photoinduced electrons from photocatalyst to target species with regard to a conventional photocatalytic process. In addition, charging of Pt is important for its catalytic ability and negatively charged Pt can weaken the molecular bond of accreted species.

3.3. H_2O/Pt/$SrTiO_3$:Nb

Evaluation of Fukui functions is helpful for understanding the intrinsic reactivity of metal adsorbed on oxide surface [61,62]. In the current work, local reactivity of Pt on the SrO-termination can be obtained by examining the Fukui functions. In general, for a system with N electrons, the two Fukui functions are

$$F^+(\mathbf{r}) = n_{N+1}(\mathbf{r}) - n_N(\mathbf{r})$$

$$F^-(\mathbf{r}) = n_N(\mathbf{r}) - n_{N-1}(\mathbf{r})$$

where n_N, n_{N+1} and n_{N-1} represent the ground-state density of system with N, $N+1$, and $N-1$ electrons, respectively. n_{N+1} and n_{N-1} are calculated at the same external potential with that of n_N, in other words, with the same geometric structure as the neutral reference system. Fukui functions provide a measurement of the change in chemical potential as the number of electrons changes. Regions where $F^+(\mathbf{r})$ is large will stabilize the uptake of charge from electron donors, while regions with high $F^-(\mathbf{r})$ will readily donate charge to electron acceptors. The Fukui functions for Pt atom adsorbed (0 0 1) surface are depicted in Fig. 8, from which it can be seen that Fukui functions are highly localized on the two side of Pt atom along the Pt–O direction. Therefore, the supported Pt atom is readily not only to withdraw charge from donor species; but also to transfer charge to acceptor species. It means that Pt acts as a reduction site when it is negatively charged. The role of Pt in mediating electron transfer from the $SrTiO_3$ to acceptor (for example, H_2O) can be significantly addressed from the Fukui functions.

In a photocatalytic water splitting reaction, photogenerated electrons and holes can migrate to the photocatalyst surface and reduce H^+ to H_2 and oxidize H_2O to O_2 [11]. In the present work, we substitute H_2O for H^+ as an acceptor to study the Pt-mediated charge transfer to give a qualitative description.

When a single Pt atom is pre-adsorbed on the Nb-doped $SrTiO_3$ (0 0 1) surface with SrO-termination, H_2O can be molecularly adsorbed on the Pt atom. The energetically most stable configuration (refer to Fig. 9, denoted as H_2O/Pt/$SrTiO_3$:Nb) indicates the adsorption energy of −0.813 eV. It should be mentioned that H_2O adsorption energy on Pt/$SrTiO_3$ (H_2O/Pt/$SrTiO_3$) is calculated to be −0.919 eV. Decreased adsorption energy is in line with downward shift of Pt *d*-band center. Again, H_2O adsorption is sensitive to the charge state of Pt. It need not compare the adsorption energies for H_2O on the SrO-termination with and without Pt, we just use molecule H_2O as a chemical probe to inspect the metal-mediated charge transfer. Since H and O readily recombine as hydroxyl on the SrO-termination, loading metal Pt on the surface may improve the H^+ yielding. For H_2O/Pt/$SrTiO_3$:Nb, charge density difference is shown in Fig. 9, from which it can be noticed the bonding between Pt and O atom of H_2O with the bond length of 2.146 Å. Distance between Pt and

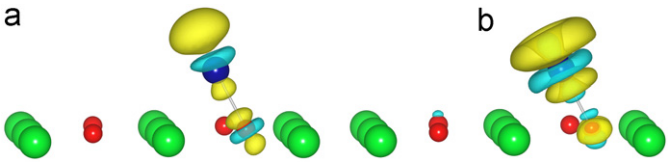

Fig. 8. Fukui functions of (a) $F^+(\mathbf{r})$; and (b) $F^-(\mathbf{r})$ of Pt on the SrO-terminated $SrTiO_3$ (0 0 1) surface (Pt/$SrTiO_3$). Cyan and yellow region, respectively, represents negative and positive function, and isosurface value is 0.002 e/Å^3. Only the first layer (SrO) of the slab is shown. (For interpretation of the references to color in this figure legend, the reader is referred to the web version of this article.)

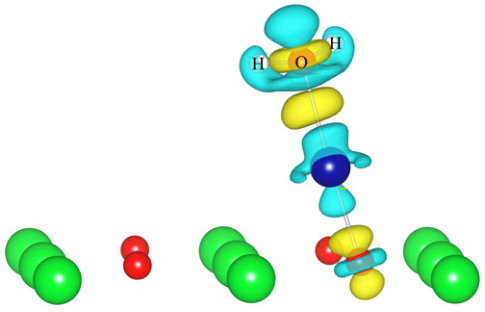

Fig. 9. Charge density difference of H_2O adsorption on Pt atom supported on (0 0 1) surface with SrO-termination of Nb-doped $SrTiO_3$ (H_2O/Pt/$SrTiO_3$:Nb); isosurface value is 0.003 e/Å^3. The cyan region represents charge depletion and the yellow region represents charge accumulation. Only the first layer (SrO) of the slab is shown and the molecule H_2O is labeled. (For interpretation of the references to color in this figure legend, the reader is referred to the web version of this article.)

surface O atom is 1.956 Å, which is shorter than that in Pt atom adsorption on Nb-doped (0 0 1) surface, 2.043 Å. When a H_2O molecule is adsorbed on Pt, charge transfer channel of –O–Pt–O– is established. Charge is transferred from electronically excited (electron-doped) $SrTiO_3$ to water, which is mediated by the Pt atom. The transferred charge is mainly localized on the O atom of molecule H_2O. There also some charge accumulates at the region between Pt and H_2O indicating that the Pt–O bond is characterized in some covalent. The H–O bond lengths in adsorbed H_2O are 0.977 and 0.982 Å, which are somewhat longer than that in the H_2O molecule in gas-phase, 0.973 Å. This is an indication that the H–O bonds are activated due to the charge transfer.

In the last place, there are also some open subjects to be resolved, for instance, the most favorable Pt nanoparticles size on $SrTiO_3$ surface and the sensitivity of molecule adsorption to the Pt nanoparticles size as well as the charge state. However, our work is of fundamental importance to understand the H_2O adsorption, metal adsorption, and the charge transfer from excited photocatalyst to adsorbate via precipitated metal with respect to the electronic excitation in a photocatalyst.

4. Conclusions

In summary, employing the first-principles DFT calculations, we studied adsorption and dissociation of H_2O on $SrTiO_3$, atomic Pt adsorption on $SrTiO_3$ and $SrTiO_3$:Nb as well as H_2O adsorption on Pt/$SrTiO_3$:Nb. The following conclusions are remarked:

(1) H_2O dissociative adsorption is more stable than molecular adsorption and intact H_2O molecule can hardly exist on the SrO-termination. H and O atoms recombine readily on this surface.
(2) Pt prefers to bond a surface O atom and intraunit polarization contributes to the Pt–O bonding. Pt adsorption introduces surface dipole moment and changes the surface work function.
(3) Charge transfer from $SrTiO_3$:Nb to Pt has been identified. Electron trapping center role Pt played on photocatalyst surface can be addressed from Pt adsorption on $SrTiO_3$:Nb.
(4) Pt mediates readily charge transfer from the surface to target species (such as H_2O) adsorbed thereon.
(5) Pt-mediated charge transfer from electron-doped $SrTiO_3$ to molecule H_2O has been identified.

Acknowledgments

This work is supported by the National Basic Research Program of China (973 program, Grant 2007CB613302), National Natural Science Foundation of China under Grants 20973102 and 11174180, and Natural Science Foundation of Shandong Province under Grant ZR2011AM009.

References

[1] M. Miyauchi, M. Takashio, H. Tobimatsu, Langmuir 20 (2004) 232.
[2] Y. Matsumoto, H. Koinuma, T. Ohsawa, J. Phys. Chem. C 111 (2007) 10523.
[3] T. Puangpetcha, T. Sreethawonga, S. Yoshikawab, S. Chavadej, J. Mol. Catal. A: Chem. 287 (2008) 70.
[4] L. Chen, S. Zhang, L. Wang, D. Xue, S. Yin, J. Cryst. Growth 311 (2009) 735.
[5] Y. Liu, L. Xie, Y. Li, R. Yang, J. Qu, Y. Li, X. Li, J. Power Sources 183 (2008) 701.
[6] X.M. Zhang, K.F. Huo, L.S. Hu, Z.W. Wu, P.K. Chuw, J. Am. Ceram. Soc. 93 (2010) 2771.
[7] D.F. Wang, T. Kako, J.H. Ye, J. Am. Chem. Soc. 130 (2008) 2724.
[8] D.F. Wang, J.H. Ye, T. Kako, T. Kimura, J. Phys. Chem. B 110 (2006) 15824.
[9] D.F. Wang, T. Kako, J.H. Ye, J. Phys. Chem. C 113 (2009) 3785.
[10] Y. Sasaki, H. Nemoto, K. Saito, A. Kudo, J. Phys. Chem. C 113 (2009) 17536.
[11] T. Puangpetch, T. Sreethawong, S. Yoshikawac, S. Chavadej, J. Mol. Catal. A: Chem. 312 (2009) 97.
[12] Y. Li, X.P. Gao, G.R. Li, G.L. Pan, T.Y. Yan, H.Y. Zhu, J. Phys. Chem. C 113 (2009) 4386.
[13] M. Miyauchi, A. Nakajima, A. Fujishima, A. Hashimoto, T. Watanabe, Chem. Mater. 12 (2000) 3.
[14] R. Konta, T. Ishii, H. Kato, A. Kudo, J. Phys. Chem. B 108 (2004) 8992.
[15] J. Wang, S. Yin, M. Komatsu, T. Sato, J. Eur. Ceram. Soc. 25 (2005) 3207.
[16] T. Ohno, T. Tsubota, Y. Nakamura, K. Sayama, Appl. Catal. A: Gen. 288 (2005) 74.
[17] H. Irie, Y. Maruyama, K. Hashimoto, J. Phys. Chem. C 111 (2007) 1847.
[18] W. Wei, Y. Dai, H. Jin, B.B. Huang, J. Phys. D: Appl. Phys. 42 (2009) 055401.
[19] W. Wei, Y. Dai, M. Guo, L. Yu, B.B. Huang, J. Phys. Chem. C 113 (2009) 15046.
[20] X.Z. Li, F.B. Li, Environ. Sci. Technol. 35 (2001) 2381.
[21] (a) P. Wang, B.B. Huang, X.Y. Qin, X.Y. Zhang, Y. Dai, J.Y. Wei, M.-H. Whangbo, Angew. Chem. Int. Ed. 41 (2008) 7931;
(b) P. Wang, B.B. Huang, X.Y. Zhang, X.Y. Qin, H. Jin, Y. Dai, Z.Y. Wang, J.Y. Wei, J. Zhan, S.Y. Wang, J.P. Wang, M.-H. Whangbo, Chem. Eur. J. 15 (2009) 18212;
(c) P. Wang, B.B. Huang, Z.Z. Lou, X.Y. Zhang, X.Y. Qin, Y. Dai, Z.K. Zheng, X.N. Wang, Chem. Eur. J. 16 (2010) 538;
(d) P. Wang, B.B. Huang, Q. Zhang, X. Zhang, X. Qin, Y. Dai, J. Zhan, J. Yu, H. Liu, Z.Z. Lou, Chem. Eur. J. 16 (2010) 10042.
[22] X. You, F. Chen, J. Zhang, M. Anpo, Catal. Lett. 102 (2005) 247.
[23] Y. Mizukoshi, Y. Makise, T. Shuto, J. Hu, A. Tominaga, S. Shironita, S. Tanabe, Ultrason. Sonochem. 14 (2007) 387.
[24] J.J. Zou, H. He, L. Cui, H.Y. Du, J. Hydrogen Energy 32 (2007) 1762.
[25] J.J. Zou, C.J. Liu, K.L. Yu, D.G. Cheng, Y.P. Zhang, F. He, H.Y. Du, L. Cui, Chem. Phys. Lett. 400 (2004) 520.
[26] F.C. Wang, C.H. Liu, C.W. Liu, J.H. Chao, C.H. Lin, J. Phys. Chem. C 113 (2009) 13832.
[27] K. Sayama, K. Mukasa, R. Abe, Y. Abe, H. Arakawa, J. Photochem. Photobiol. A: Chem. 148 (2002) 71.
[28] V. Subramanian, E.E. Wolf, P.V. Kamat, J. Am. Chem. Soc. 126 (2004) 4943.
[29] Z. Shan, J. Wu, F. Xu, F. Huang, H. Ding., J. Phys. Chem. C 112 (2008) 15423.
[30] Q. Jiang, J. Zegenhagen, Surf. Sci. 367 (1996) L42.
[31] N. Erdman, O. Warschkow, M. Asta, K.R. Poeppelmeier, D.E. Ellis, L.D. Marks, J. Am. Chem. Soc. 125 (2003) 10050.
[32] G. Charlton, S. Brennan, C.A. Muryn, R. McGrath, D. Norman, T.S. Turner, G. Thornton, Surf. Sci. 457 (2000) L376.
[33] E. Erdman, K.R. Poeppelmeier, M. Asta, O. Warschkow, D.E. Ellis, L.D. Marks, Nature 419 (2002) 55.
[34] R.A. Evarestov, A.V. Bandura, V.E. Alexandrov, Surf. Sci. 601 (2007) 1844.
[35] H.L. Zhang, G. Chen, Z.H. Li, Appl. Surf. Sci. 253 (2007) 8345.
[36] M. Cai, Y. Zhang, G. Yang, Z. Yin, M. Zhang, W. Hu, Y. Wang, J. Chem. Phys. 124 (2006) 174701.
[37] W. Wei, Y. Dai, M. Guo, Y.T. Zhu, B.B. Huang, J. Phys. Chem. C 114 (2010) 10917.
[38] Y.X. Wang, M. Arai, T. Sasaki, C.L. Wang, Phys. Rev. B 73 (2006) 035411.
[39] T. Sakata, K. Hashimoto, T. Kawai, J. Phys. Chem. 88 (1984) 5214.
[40] D.S. Shang, J.R. Sun, L. Shi, B.G. Shen, Appl. Phys. Lett. 93 (2008) 102106.
[41] T. Susaki, Y. Kozuka, Y. Tateyama, H.Y. Hwang, Phys. Rev. B 76 (2007) 155110.
[42] Y.M. Cui, R.M. Wang, Appl. Phys. Lett. 91 (2007) 233513.
[43] T. Shimizu, H. Okushi, J. Appl. Phys. 85 (1999) 7244.
[44] W. Wei, Y. Dai, M. Guo, L. Yu, H. Jin, S.H. Han, B.B. Huang, Phys. Chem. Chem. Phys. 12 (2010) 7612.
[45] G. Kresse, J. Furthmuller, Comput. Mater. Sci. 6 (1996) 15.
[46] G. Kresse, J. Furthmuller., Phys. Rev. B 54 (1996) 11169.
[47] P.E. Blöchl, Phys. Rev. B 50 (1994) 17953.
[48] J.P. Perdew, Y. Wang, Phys. Rev. B 45 (1992) 13244.
[49] J.P. Perdew, K. Burke, M. Ernzerhof, Phys. Rev. Lett. 77 (1996) 3865.
[50] S. Piskunov, E.A. Kotomin, E. Heifets, J. Maier, R.I. Eglitis, G. Borstel, Surf. Sci. 575 (2005) 75.
[51] J.L. Wang, M. Fu, X.S. Wu, D.M. Bai, J. Appl. Phys. 105 (2009) 083526.
[52] O. Nakagawara, M. Kobayashi, Y. Yoshino, Y. Katayama, H. Tabata, T. Kawai, J. Appl. Phys. 78 (1995) 7226.
[53] J. Neugebauer, M. Cheffler, Phys. Rev. B 46 (1992) 16067.
[54] G. Henkelman, B.P. Uberuaga, H.J. Jonsson, Chem. Phys. 113 (2000) 9978.
[55] F. Lin, F.W. Zheng, F.P. Ouyang, Acta Phys. Sin. 58 (2009) S193.
[56] K. Iwahori, S. Watanabe, M. Kawai, K. Kobayashi, H. Yamada, K. Matsushige, J. Appl. Phys. 93 (2003) 3223.
[57] A. Asthagiri, D.S. Sholl, J. Chem. Phys. 116 (2002) 9914.
[58] K. Mitsuhara, Y. Kitsudo, H. Matsumoto, A. Visikovskiy, M. Takizawa, T. Nishimura, T. Akita, Y. Kido, Surf. Sci. 604 (2010) 548.
[59] W.X. Li, C. Stampfl, M. Scheffler, Phys. Rev. B 65 (2002) 075407.
[60] Z. Zeng, J.L.F.D. Silva, H.Q. Deng, W.X. Li, Phys. Rev. B 79 (2009) 205413.
[61] L.M. Molina, J.A. Alonso, J. Phys. Chem. C 111 (2007) 6668.
[62] P.W. Ayers, R.G. Parr, J. Am. Chem. Soc. 122 (2000) 2010.